



Published in final edited form as:

Nature. 2019 October ; 574(7780): 717–721. doi:10.1038/s41586-019-1700-7.

ALCOHOL METABOLISM CONTRIBUTES TO BRAIN HISTONE ACETYLATION

P Mews^{1,2,*}, G Egervari^{1,*#}, R Nativio¹, S Sidoli^{1,3}, G Donahue¹, SI Lombroso¹, DC Alexander¹, SL Riesche¹, EA Heller¹, EJ Nestler², BA Garcia¹, SL Berger^{1,#}

¹ Epigenetics Institute, Perelman School of Medicine at the University of Pennsylvania, Philadelphia, PA, United States

²Icahn School of Medicine at Mount Sinai, Fishberg Department of Neuroscience, New York, NY, United States

³Current affiliation: Department of Biochemistry, Albert Einstein College of Medicine, New York, NY, United States

Abstract

Emerging evidence suggests that epigenetic regulation is dependent on metabolic state, implicating specific metabolic factors in neural functions that drive behavior¹. In neurons, histone acetylation relies on the metabolite acetyl-CoA that is produced from acetate by chromatin-bound acetyl-CoA synthetase 2 (ACSS2)². Notably, a major source of acetate is via breakdown of alcohol in the liver, leading to rapidly increasing blood acetate³. Neuronal histone acetylation may thus be under the influence of alcohol-derived acetate⁴, with potential effects on alcohol-induced brain gene expression and behavior⁵. Here, using *in vivo* stable isotope labeling in mouse, we show that alcohol metabolism contributes to rapid histone acetylation in the brain in part by direct deposition of alcohol-derived acetyl groups onto histones in an ACSS2-dependent manner. A similar induction was observed with heavy labeled acetate injection *in vivo*. In a pregnant mouse, exposure to labeled alcohol resulted in incorporation of labeled acetyl groups into gestating fetal brains. In isolated primary hippocampal neurons *ex vivo*, extracellular acetate induced learning and memory-related transcriptional programs that were sensitive to ACSS2 inhibition. Notably, we

Users may view, print, copy, and download text and data-mine the content in such documents, for the purposes of academic research, subject always to the full Conditions of use:http://www.nature.com/authors/editorial_policies/license.html#terms

#Corresponding authors Correspondence should be addressed to Shelley Berger (bergers@penmedicine.upenn.edu) and Gabor Egervari (egervari@penmedicine.upenn.edu).

*authors contributed equally

Author Contributions

P.M. and S.L.B. developed the primary hypothesis. P.M., G.E. and S.L.B. designed the project. P.M. and G.E. performed most of the experiments. P.M. planned the d6-EtOH labeling mass spectrometry, performed together with R.N., G.E., and S.S.. G.E. and S.S. performed the d3-acetate labeling mass spectrometry. The RNA-seq was performed *in vivo* by P.M. and *in vitro* by G.E., with support from R.N.. R.N. conducted the ChIP-seq. G.D. analysed all ChIP-seq and RNA-seq datasets. G.E., S.I.L., D.C.A. and E.A.H. performed the behavioral characterization. P.M. performed the labeling experiments for metabolomic analysis. The fetal alcohol labeling was done by G.E., with support from S.L.R.. P.M., G.E., and S.L.B. wrote the manuscript. All authors reviewed the manuscript and discussed the work.

Competing interests

The authors declare no competing financial interests.

Data availability

All RNAseq and ChIPseq data are available at GEO SuperSeries GSE122188. Raw mass spectrometry data are provided as Extended Data Table 2.

showed that alcohol-related associative learning requires ACSS2 *in vivo*. These findings support a direct link between alcohol metabolism and gene regulation through ACSS2-dependent histone acetylation in the brain.

To determine whether acetate from alcohol breakdown contributes to dynamic histone acetylation in the brain, we employed *in vivo* stable isotope labeling of protein acetylation monitored by mass spectrometry (MS) (Fig. 1a)⁶. EtOH-derived acetyl-groups were rapidly incorporated into histone acetylation in the brain, both in hippocampus (Fig. 1b) and in prefrontal cortex (Extended Data Fig. 1c). Label incorporation into histone acetylation was dynamic in hippocampus and heavy labeling decreased to baseline levels 8 hours following i.p. injection (Extended Data Fig. 2a–b). This rapid *in vivo* labeling of hippocampal histone acetylation was absent in mice injected with non-labeled alcohol (Extended Data Fig. 2d). Similar labeling occurred in the liver (Fig. 1c), which is the principal site of alcohol metabolism and expresses high levels of ACSS2^{7,8}. In contrast, lower labeling of histone acetylation was observed in skeletal muscle (m. gastrocnemius, Extended Data Fig. 1d, 2e), which expresses relatively lower levels of ACSS2⁹.

To test whether ACSS2 is required for the brain incorporation of acetate derived from alcohol, we attenuated ACSS2 expression in the dorsal hippocampus (dHPC) by shRNA knockdown using a previously validated viral vector². In these ACSS2 knockdown (KD) animals, we compared heavy-alcohol-derived histone acetylation separately in the dHPC, where ACSS2 was reduced (ACSS2 KD), and in the ventral hippocampus (vHPC), where ACSS2 was not targeted by injection. Strikingly, ACSS2 KD prevented the incorporation of alcohol-derived heavy acetyl groups into histone acetylation (Fig. 2a). In contrast, in the same animal, vHPC incorporation of the heavy label was not affected (Fig. 2b). These *in vivo* data indicate that acetate derived from hepatic alcohol metabolism is transported to the brain and readily incorporated into ACSS2-dependent histone acetylation (see further discussion in Supplemental Information).

Notably, even though the bulk of alcohol metabolism takes place in the liver, alcohol fractions may also be converted to acetate in the brain via the enzymes catalase and CYP2E1¹⁰. We therefore assessed the contribution of extracellular acetate-derived acetyl groups to histone acetylation in the brain. In mice intraperitoneally injected with 2 g/kg deuterated acetate (d3-acetate), we detected rapid label incorporation into brain histone acetylation, at similar levels in both hippocampus and cortex (Extended Data Fig. 2f,g). Relative labeling was highest at 30 minutes and returned to background levels at 4 hours post-injection, indicating rapid incorporation of acetate-derived acetyl groups as well as rapid turnover of brain histone acetylation. Notably, we found that acetate levels in the hippocampus were significantly increased at 30 minutes after alcohol injection, or following acetate injection (Extended Data Fig. 2h), and detected substantial amounts of heavy acetate in the hippocampus as early as 30 minutes following injection with d6-EtOH (Extended Data Fig. 3a).

We further investigated whether alcohol-derived carbons are incorporated into other key metabolites in hippocampal tissue. While we detected no label incorporation into glucose and 3-hydroxybutyrate, and only a fraction into lactate pools (<1%), we found that alcohol

labels glutamine pools in the hippocampus (Extended Data Fig. 3b–e). In the brain, *de novo* synthesis of glutamine occurs in astrocytes and replenishes the glutamate-glutamine cycle, as it is trafficked into glutamatergic neurons for production of the neurotransmitter glutamate. Citrate – the substrate used by ATP-citrate lyase (ACL) to produce nucleocytoplasmic acetyl-CoA – is generated from α -ketoglutarate that can derive from carboxylation of glutamine; this path could provide another route for alcohol to contribute to histone acetylation. However, we detected only traces of alcohol-derived label in hippocampal citrate/isocitrate pools (Extended Data Fig. 3f). Taken together with our mass spec in ACSS2 KD animals (Fig. 2a,b), these results support the view that alcohol-derived acetate contributing to hippocampal histone acetylation is converted directly by ACSS2. Accordingly, our data suggest that increased blood acetate from alcohol metabolism promotes ACSS2-mediated dynamic histone acetylation in the brain.

We examined the functional relevance of alcohol-derived acetate for ACSS2-dependent histone acetylation in regulating hippocampal gene expression. We found that alcohol administration in WT mice resulted in significant enrichment of H3K9ac and H3K27ac peaks at key neuronal genes and genome-wide, and this enrichment was greatly attenuated in the ACSS2 KD (Fig. 2c–g; ChIP-seq performed 1 hour after alcohol injection). For example, we observed ACSS2-dependent and alcohol-induced histone acetylation at *Fstl1* (follistatin-like 1; Fig. 2c), a neuronal gene that has been implicated in neuronal development and migration¹¹. We observed alcohol-induced H3K27ac at *Cep152* (centrosomal protein of 152 kDa) gene (Extended Data Fig.4a), an important regulator of genome integrity that is recurrently mutated in intellectual developmental disorders and microcephaly¹². Another example is the *Uimc1* (ubiquitin interaction motif containing 1) gene (Extended Data Fig. 4b), previously connected to neurodevelopmental disorders and autism¹³. Evaluating the histone acetylation ChIP-Seq genome-wide, we found that 74% of H3K9ac peaks changed upon alcohol exposure were increased (339 out of 458 changed peaks called with MACS2, using 10% FDR significance threshold for DiffBind; Fig. 2d), and that 60% of differential H3K27ac peaks were increased by ethanol (490 out of 816 peaks, Fig. 2e; ChIP-seq performed 1 hour after alcohol injection). Strikingly, this response was eliminated in ACSS2 KD animals – 98% of H3K9ac and H3K27ac peaks increased in WT failed to induce upon EtOH treatment in the dHPC (Fig. 2f,g). We then performed RNA-seq to characterize the transcriptional response and found that H3K9ac and H3K27ac drove gene expression in EtOH-treated WT animals genome-wide (Extended Data Fig. 5a,b). However, in line with the ChIP-seq data, this response was blunted in ACSS2 KD mice (Extended Data Fig. 5c,d). Functional analysis of genes that were both hyperacetylated and induced by EtOH in an ACSS2-dependent manner included enrichment in genes with functions in protein binding, cell junction, postsynaptic density, and response to drug (Extended Data Fig. 5e,f). Together, our *in vivo* findings show that alcohol administration leads to increased histone acetylation and transcriptional activity in the dHPC in an ACSS2-dependent manner.

Because alcohol and acetate have pleiotropic effects on brain circuitry and metabolism¹⁴, we then developed an *ex vivo* assay to more closely model the direct effects of exogenous acetate on gene expression. We utilized isolated mouse primary hippocampal neurons to investigate the transcriptional response to supraphysiological levels of acetate (cells were cultured for one week after isolation and subsequently treated with 5 mM acetate for 24

hours) that mimics exogenous acetate influx during alcohol intake. Further, to determine the specific role of ACSS2 in transcriptional responses to acetate, we employed a highly specific small molecule inhibitor of ACSS2 (ACSS2i; C20H18N4O2S2, Extended Data Fig. 6a)^{2,7}.

In primary hippocampal neurons, acetate supplementation induced 3613 genes (Fig. 3a, Extended Data Fig. 6b) that were, via Gene Ontology (GO) term analysis, involved in nervous system processes, including signal transduction and learning and memory (Extended Data Fig. 6c). In contrast, acetate treatment resulted in down regulation of genes involved in immune system processes (Extended Data Fig. 6d). In the presence of the ACSS2i, 2107 of the acetate-induced genes failed to become upregulated (Extended Data Fig. 6f), indicating that acetate-induced transcription relies heavily on the catalytic activity of ACSS2. Importantly, acetate-induced genes were not regulated by ACSS2i treatment in the absence of acetate (uninduced right boxes in Extended Data Fig. 6e). GO analysis of ACSS2i-sensitive upregulated genes showed enrichment for nervous system processes, behavior, and learning and memory (Extended Data Fig. 6f) and specific genes showed ACSS2i sensitivity (Extended Data Figs. 7a–d). For example, *Slc17a7* was upregulated upon acetate treatment in WT hippocampus cells but induction was diminished when ACSS2 was inhibited (Extended Data Fig. 7a). *Slc17a7* encodes vesicular glutamate receptor 1 (Vglut1), implicated in hippocampal synaptic plasticity, addiction and alcohol use¹⁵. In addition, impaired DNA methylation of *Ccnj1* (Cyclin J-like) has been linked to prenatal alcohol exposure and FASD¹⁶ (Extended Data Fig. 7b). Further analysis revealed that the ACSS2i-sensitive and acetate-upregulated genes were also bound by hippocampal ACSS2 (our previous ChIP-seq²), and binding was promotor-proximal at baseline without any direct behavioral stimulation *in vivo*² (Extended Data Fig. 8a). GO analysis linked these ACSS2 target genes to intricate plasticity-related mechanisms involving axonogenesis and voltage-gated ion channel activity (Fig. 3b). Correspondingly, motif analysis of ACSS2-targeted, acetate-induced, and ACSS2i-sensitive genes implicated the involvement of neuronal transcription factors – including E2F3 and NR5A2 (Fig. 3c) – linked to neurodifferentiation and the regulation of behavior by drugs of abuse^{17,18}.

Notably, there was substantial overlap of genes that were upregulated by alcohol *in vivo* in dorsal hippocampus and genes that were induced by acetate *ex vivo* (RNA-seq found 830 alcohol-responsive hippocampal genes to overlap with the *ex vivo* differentially expressed genes; Fig. 3d), supporting the translational validity of our *ex vivo* model. GO analysis for these overlapping genes indicated enrichment of genes related to neuronal plasticity, including synapse, neuron projection, and axons, but also ribosomal and mitochondrial functions (Extended Data Fig. 8b). Notably, a previously published microarray data set of *in vivo* alcohol-regulated hippocampal genes also showed substantial overlap with our list of *ex vivo* acetate-induced genes (38% of 214 alcohol-responsive hippocampal genes in the microarray¹⁹). Next, we showed – starting from our *in vivo* data in a complementary analysis – that ACSS2 target genes with alcohol-induced H3K9ac in hippocampus *in vivo* were also upregulated by acetate treatment of hippocampal neurons *ex vivo*, and that ACSS2i blocks this gene induction (Fig. 3e). The equivalent relationship existed for hippocampal genes with alcohol-induced H3K27ac *in vivo*, which failed to be induced by acetate *ex vivo* in the presence of ACSS2i (Fig 3f).

Together, these findings suggest that ACSS2 may play a role in alcohol-related learning via coordinating alcohol-induced histone acetylation and gene expression. To examine potential behavioral effects in WT and ACSS2 KD mice, we performed ethanol-mediated conditioned place preference (CPP), which has been previously used to assess ethanol-associated learning²⁰. In this paradigm, animals are exposed to neutral and rewarding stimuli in distinct spatial compartments, distinguished by environmental cues. After conditioning, CPP is measured by allowing the animals free access to either compartment and measuring time spent in the reward-associated chamber (Fig. 4a). To assess place preference learning, we calculated mean time spent in the conditioned and unconditioned chambers (Extended Data Fig. 9c) as well as a CPP score, which we defined as the difference between time spent in the conditioned versus the unconditioned chamber (Fig 4b). We found that WT mice spent increased time in the compartment in which ethanol was delivered during training (Wilcoxon, $p=0.0391$, Fig. 4b). Importantly, acquisition of CPP depends on dorsal HPC (dHPC) spatial memory formation, and, accordingly, dorsal HPC lesions disrupt place conditioning²¹. To test the importance of ACSS2 in the dHPC, we used GFP-expressing lentivirus mediated shRNA knock down to reduce the protein level of ACSS2 ($n=10$) compared to control shRNA ($n=8$; Extended Data Fig. 9a,b). We observed a significant main effect of the conditioning subgroup ($p=0.0227$; $F_{1,32}=5.731$; main effect of “training” from 2-way ANOVA across the 4 groups) showing that the ethanol-induced CPP procedure was successful. Importantly, we also observed a significant treatment x conditioning subgroup interaction ($p=0.0462$; $F_{1,32}=4.303$; interaction from 2-way ANOVA across the 4 groups), indicating that the treatment variable (i.e. the dorsal hippocampal ACSS2 KD) significantly reduced the expression of CPP. Strikingly, we found that ethanol-associated CPP was abolished in ACSS2 KD (dHPC) mice (Wilcoxon, $p=0.4316$, Fig. 4b), indicating that ethanol-related associative memory formation requires ACSS2.

Taken together, the *ex vivo* and *in vivo* molecular data, along with the behavioral findings, show that ACSS2 is required for heavy labeled acetate incorporation into acetylated histones in the dorsal HPC, which facilitates memory-related gene expression and alcohol-related associative learning (Fig. 4c). These results establish ACSS2 as a promising candidate for therapeutic intervention in alcohol use disorders, in which memory of alcohol-associated environmental cues is a primary driver of craving and relapse even after protracted periods of abstinence.

Importantly, alcohol exposure not only disrupts epigenetic and transcriptional processes in the adult brain but is also linked to epigenetic dysregulation in the gestating fetus²². *In utero*, alcohol is an environmental teratogen that affects neuro-developmental gene expression and can elicit numerous alcohol-associated postnatal disease phenotypes that together are categorized as fetal alcohol spectrum disorder (FASD)²³. Recent investigations of alcohol-mediated epigenetic changes *in utero* have implicated altered histone acetylation in FASD²⁴, but the underlying mechanisms are unknown.

We investigated whether alcohol affects dynamic histone acetylation *in utero* in the developing fetal mid- and forebrain (E18.5). Fetal brain MS showed that ‘binge drinking-like’ alcohol exposure – parallel to maternal labeling of neuronal histone acetylation – resulted in deposition of alcohol-derived acetyl-groups onto histones in fetal fore- and

midbrain in early neural development (Fig. 4e; Extended Data Fig. 9d), indicating an unanticipated potential mechanism for FASD etiology.

In the adult brain, epigenetic mechanisms that control gene expression play a key role in processing neural activity to continuously adapt circuit connectivity and behavior^{25,26}. Here, we show that alcohol exposure gives rise to brain histone acetylation both directly, by way of direct incorporation of alcohol-derived acetate, as well as indirectly, by utilizing other metabolic pathways. Incorporation of alcohol-derived acetate into histone acetylation was recently observed in the liver²⁷. However, to our knowledge, our data provide the first empirical evidence indicating that a portion of acetate derived from alcohol metabolism directly influences epigenetic regulation in the brain. We show that this direct pathway has important functional and behavioral consequences that illuminate a novel neurobiological aspect of alcohol use. Considering the exceedingly complex effects of ethanol on the brain and behavior, further studies will be required to determine the relative contributions of ethanol-derived histone acetylation, ethanol-induced intracellular signaling pathways, and ethanol-related redox stress. We further show that brain histone acetylation is via acetyl-CoA generation by metabolic ACSS2. In the hippocampus, alcohol-derived acetyl group incorporation may be of critical importance for alcohol-related associative learning, which encodes environmental cues associated with alcohol that drive craving, seeking, and consumption even after protracted periods of abstinence. This novel and direct pathway substantially furthers our understanding of alcohol-induced epigenetic regulation in the brain, which was hitherto limited to indirect effects of alcohol-induced intracellular signaling and changes in the expression or activity of histone modifying enzymes. This direct link contributes to a large proportion of histone acetylation following ethanol use and signifies a strong physiological relevance of direct incorporation, which we show contributes to transcriptional and behavioral adaptations induced by ethanol. Importantly, these findings suggest that other peripheral sources of physiological acetate – primarily the gut microbiome – may similarly affect central histone acetylation and brain function, which may either control or foster other metabolic syndromes. Translational treatment strategies that target this nexus between peripheral metabolic activity and neuro-epigenetic regulation may pave the way for novel therapeutic interventions for alcohol use and other neuropsychiatric disorders.

Supporting information for publication

Stable isotope labeling of brain histone acetylation

We injected mice intraperitoneally with 2 g/kg deuterated ethanol (d6-EtOH) or control saline, and assessed deuterium incorporation into acetylated histones at baseline, as well as at 1 and 4 hours after intraperitoneal injections (Fig 1a). We confirmed that the injected d6-EtOH is readily metabolized to acetate that becomes systemically accessible (Extended Data Fig. 1a), resulting in rapid labeling of blood acetate (Extended Data Fig. 1b). Using advanced quantitative liquid chromatography-MS technology, we quantified the relative abundance of isotopically labeled histone acetylation in the brain and in peripheral tissues (Fig. 1a, right panels). Analysis of the heavy labeling patterns showed that heavy ethanol injection leads to marked increases of the M+3 isotope (Extended Data Fig. 1e,f;

Supplemental Table 1), which suggests that ethanol-derived acetate contributes to histone acetylation via direct deposition of triply deuterated acetyl-CoA. This increase in the M+3 isotope was also evident accounting for natural levels of heavy isotopes of carbon and hydrogen (Extended Data Fig. 1g,h; also see Methods for detailed descriptions). The increases of M+1 and M+2 isotopes (Extended Data Fig. 1h) could be driven by deuterium back exchange²⁸ or by singly and doubly deuterated metabolites, indicating that alternative metabolic pathways also contribute to histone acetylation labeling; however the major increase is to the M+3 isotope via triply deuterated acetate. Further, we performed ¹³C-labeled alcohol tracing and found rapid incorporation into hippocampal histone acetylation, equivalent to d6-EtOH (Extended Data Fig. 2c). We explored whether gestational alcohol exposure influences histone acetylation in the developing fetal brain by measuring direct deposition of alcohol-derived acetyl groups onto histones. Using the protocol described above, of heavy-labeled alcohol injections (2 mg/kg i.p.) followed by mass spectrometry on isolated histone proteins, we confirmed incorporation of alcohol metabolites (4h post-injection) into the neuronal histone acetylation in gestating female mice (Fig. 4d), consistent with the previous results in males (compare to Fig. 1b).

Histone extraction

Histones were extracted as previously described. The cells were incubated in nuclear isolation buffer (NIB) (15 mM Tris-HCl, 15 mM NaCl, 60 mM KCl, 5 mM MgCl₂, 1 mM CaCl₂, 250 mM sucrose, pH 7.5, and 0.5 mM AEBSF, 10 mM sodium butyrate, 5 nM microcystin, 1 mM DTT added fresh) with 0.2% NP-40 on ice for 5 min. The nuclei were collected by centrifuging at 700 × g at 4°C for 5 min. The resulting nuclear pellet was washed twice with the same volume of nuclear isolation buffer without NP-40. Histones were then acid-extracted with 0.2 M H₂SO₄ for 3 hours at 4°C with rotation. The insoluble nuclear debris were pelleted at 3400 × g at 4°C for 5 min, and the supernatant was retained. Next, histone proteins were precipitated by adding 100% trichloroacetic acid (TCA) in the ratio of 1:3 (v/v) for 1 hour at 4°C. The pellet was washed with acetone to remove acid residual. Histones were resuspended in 30 µl of 50 mM NH₄HCO₃ (pH 8.0).

Histone propionylation and digestion

Histones were derivatized and digested as previously described. The sample was mixed with 15 µl of derivatization mix, consisting in propionic anhydride and acetonitrile in a ratio of 1:3 (v/v), immediately followed by 7.5 µl of ammonium hydroxide to maintain pH 8.0. The sample was incubated for 15 minutes at 37°C, dried and the derivatization procedure was repeated one more time. Samples were then resuspended in 50 mM NH₄HCO₃ and incubated with trypsin (enzyme:sample ratio 1:20) overnight at room temperature. After digestion, the derivatization reaction was performed again twice to derivatize peptide N-termini. Samples were desalted using C₁₈ Stage-tips prior to LC-MS analysis.

NanoLC-MS/MS

Samples were analyzed by using a nanoLC-MS/MS setup. NanoLC was configured with a 75 µm ID x 25 cm Reprosil-Pur C18-AQ (3 µm; Dr. Maisch GmbH, Germany) nano-column using an EASY-nLC nano-HPLC (Thermo Scientific, San Jose, CA, USA), packed in-house. The HPLC gradient was as follows: 5% to 32% solvent B (A = 0.1% formic acid; B = 80%

acetonitrile, 0.1% formic acid) over 45 minutes, from 32% to 90% solvent B in 5 minutes, 90% B for 10 minutes at a flow-rate of 300 nL/min. nanoLC was coupled to an Orbitrap Elite mass spectrometer (Thermo Scientific, San Jose, CA, USA). The acquisition method was data independent acquisition (DIA) as described. Briefly, two full scan MS spectra (m/z 300–1100) were acquired in the ion trap within a DIA duty cycle, and 16 ms/ms were performed with an isolation window of 50 Da. Normalized collision energy (CE) was set to 35%.

Data Analysis

Raw MS data were analyzed manually. We selected the 7 most intense peptides of histone H3 and H4 containing acetylations, and we extracted the relative abundance of the M+1, M+2 and M+3 isotopes compared to the monoisotopic signal. The other peptides were not considered as, due to their low abundance, we could not reliably quantify the relative abundance of all the isotopes. The percentage represented in the radar plots indicates the relative intensity of the M+3 signal (the fourth isotope) as compared to the monoisotopic signal. Data were not normalized to the non-labeled sample, so that the relative abundance of the natural isotopic distribution can be appreciated also in the untreated mice.

As statistical analysis, we performed two-tails heteroscedastic t-test (significant when p -value <0.05) when comparing the same isotope in treated vs untreated samples (Supplemental Table 1). In this analysis, we considered differences in relative abundance of all isotopes (M+1, M+2, M+3), and found that major changes occur on M+3 (Supplemental Tables 1 and 2). We used *enviPat*²⁹ to estimate the theoretical relative abundance of the first four isotopes of the seven peptides considered in this study, which showed no significant difference to the observed isotopic distribution of the untreated samples (Extended Data Fig 1g). Natural abundance corrections were performed using *FluxFix*³⁰, in order to calculate the exact relative abundance of the isotopes M+1, M+2 and M+3 in the samples treated with labeled ethanol or acetate (Extended Data Fig 1h). Using a matrix-based natural abundance correction approach proposed by Fernandez et al.³¹, this calculation corrects for the contribution of each isotopologue, removing, for example, from the M+3 signal the portion of the isotopic pattern contributed by the increase of the M+1 and M+2 species.

ChIP-sequencing

ChIP-seq was performed as previously described with modifications for mouse brain preparation³². Briefly, ~20 mg dorsal hippocampus from each mouse was minced on ice and crosslinked with 1% formaldehyde for 10 min and quenched with 125 mM glycine for 5 min. Nuclei were prepared by dounce homogenization of crosslinked tissue in nuclei isolation buffer (50 mM Tris-HCl at pH 7.5, 25 mM KCl, 5 mM MgCl₂, 0.25 M sucrose) with freshly added protease inhibitors and sodium butyrate. Nuclei were lysed in nuclei lysis buffer (10 mM Tris-HCl at pH 8.0, 100 mM NaCl, 1 mM EDTA, 0.5 mM EGTA, 0.1% Na-deoxycholate, 0.5% N-lauroylsarcosine) with freshly added protease inhibitors and sodium butyrate and chromatin was sheared using a Covaris S220 sonicator to ~250 bp size. Equal aliquots of sonicated chromatin were used per immunoprecipitation reaction with 5 ul H3K9ac antibody (Active Motif, cat # 39137; lot # 09811002 or 4 ul H3K27ac antibody (Abcam, cat #4729; lot # GR323132-1) pre-conjugated to Protein G Dynabeads (Life

Technologies). 10% of the chromatin was saved as Input. ChIP reactions were incubated overnight at 4°C with rotation and washed three times in wash buffer. Immunoprecipitated DNA was eluted from the beads, reversed crosslinked and purified together with Input DNA. 10 ng DNA (either ChIP or Input) was used to construct sequencing libraries using the NEBNext Ultra II DNA library prep kit for Illumina (New England Biolabs, NEB). Libraries were multiplexed using NEBNext Multiplex Oligos for Illumina (dual index primers) and single-ended sequenced (75 bp) on the NextSeq 500 platform (Illumina) in accordance with the manufacturer's protocol.

ChIP-seq analysis

ChIP-seq tags generated with the NextSeq 500 platform were demultiplexed with the `bcl2fastq` utility and aligned to the mouse reference genome (assembly GRCm38/mm10) using Bowtie v1.1.1 allowing up to two mismatches per sequencing tag (parameters `-m 1 --best`)³³. Peaks were detected using MACS2 (tag size = 75 bp; FDR < 1×10^{-3}) from pooled H3K9ac or H3K27ac tags of mice from the same condition along with treatment-matched Input tags as control. The MTL method³⁴ was used to compare H3K9ac or H3K27ac enrichment in the four study conditions. Statistical significance of differential H3K9ac or H3K27ac enrichments was assessed by using DiffBind (Bioconductor v3.7) in a 2-way comparison (wt-saline vs wt-EtOH or ACSS2KD-saline vs ACSS2KD-EtOH) across the individual replicate samples (FDR < 10%). UCSC Genome Browser track views were created for ChIP-seq data by first pooling replicates and generating coverage maps using BEDtools `genomeCoverageBed -bg`, then adjusting for library size using the RPM coefficient. Input signal was then subtracted from ChIP signal. Resulting tracks were converted from `bedGraph` to `bigWig` using the Genome Browser's `bedGraphToBigWig` utility. RNA-seq tracks were created similarly, first splitting by tag orientation to the genomic reference strand and then creating coverage maps. Because an RPM adjustment might disguise a large deformation in the transcriptome distribution, maps were adjusted for library size using the average scalar coefficient size factor determined by DESeq2. Resulting tracks were converted to `bigWigs` as ChIP-seq tracks were, and the + and - tags from a given sample were plotted as overlays in a track hub.

RNA-sequencing

All RNA-seq data were prepared for analysis as follows: NextSeq sequencing data was demultiplexed using native apps on BaseSpace. Demultiplexed FASTQs were aligned by RNA-STAR 2.5.2 to assembly mm10 (GRCm38). Aligned reads were mapped to genomic features using HTSeq 0.6.1. Quantification, library size adjustment, and differential gene expression analysis was done using DESeq2 and Wald's test (pairwise contrasts between acetate and DMSO-treatment in the inhibitor-treated or untreated cells, followed by a set overlap of differentially expressed genes). Gene list overlaps were tested for significance using the hypergeometric test.

Functional analysis

Gene Ontology analysis was performed using DAVID with an FDR cutoff of 10%, filtering categories with fewer than 10 genes or less than 2.5X fold enrichment over background. Motif analysis was performed using HOMER v4.6 on all ACSS2 peaks from published in

vivo data² targeting (by the nearest TSS) a gene sensitive to acetate with H3K9ac at the promoter using a fixed window of 300bp².

Primary hippocampal neurons

Plated primary hippocampal neurons were obtained from the Neurons R Us neuronal core at the University of Pennsylvania. Cells were maintained in neurobasal medium (NBM; Gibco) supplemented with GlutaMAX (Gibco) and B27 (Gibco). After 7 days of differentiation, cells were treated for 24 hours with 5 mM acetate or vehicle (NBM) in the presence or absence of 20uM ACSS2 inhibitor or vehicle (DMSO diluted into NBM). Cells were lysed using QIAzol (Qiagen) and RNA was extracted using the RNeasy Mini Kit (Qiagen). RNAseq libraries were prepared using the NEBNext Ultra II Directional RNA library prep kit (NEB).

Mouse experiments

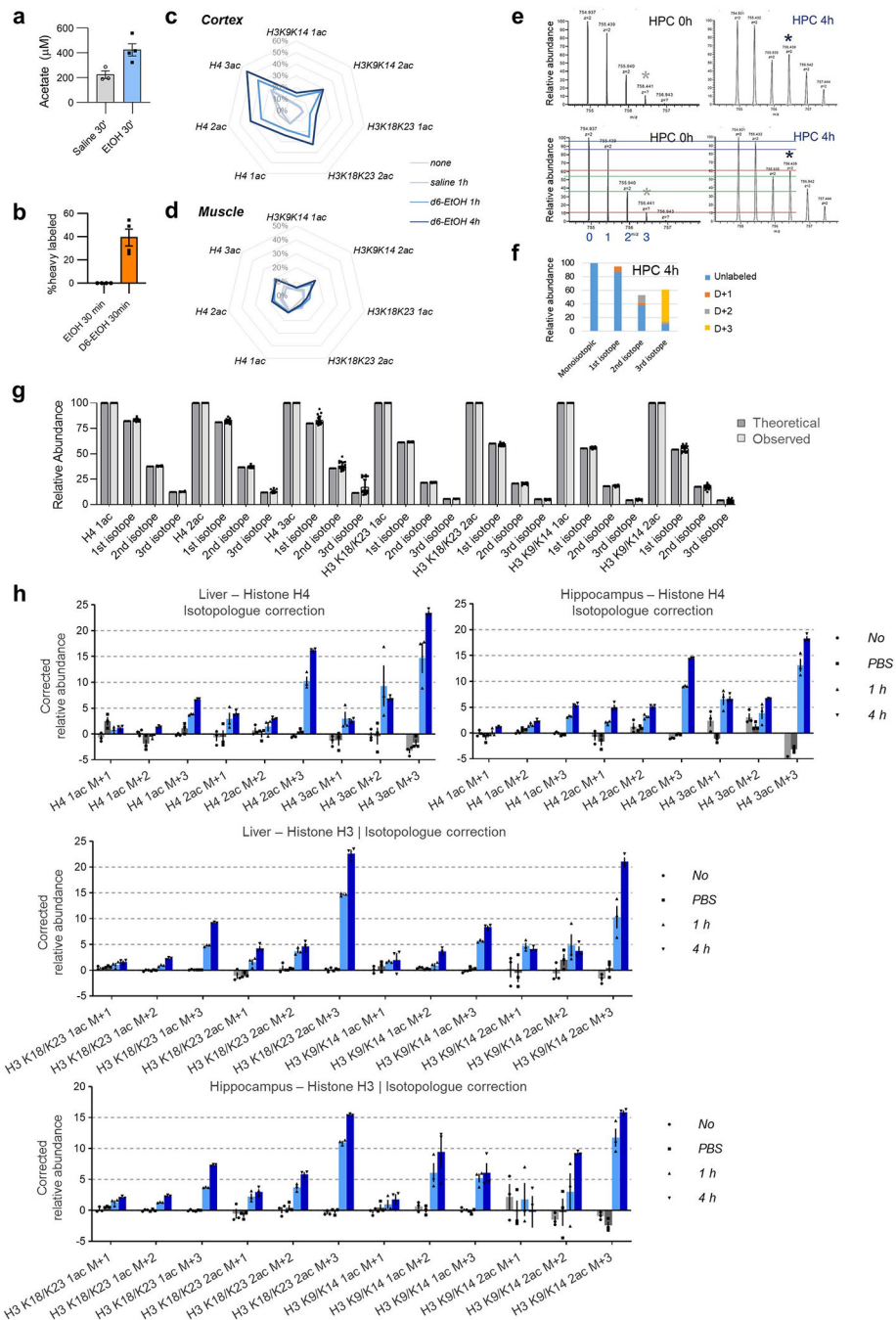
Animal use, surgical procedures, and all experiments performed were approved by the Institutional Animal Care and Use Committee (IACUC, protocol 804849). All personnel involved have been adequately trained and are qualified according to the Animal Welfare Act (AWA) and the Public Health Service (PHS) policy. 8 weeks old adult male mice or E18.5 pregnant females were used. Ethanol, ethanol-d6 (Sigma-Aldrich-186414), ethanol-1-13C (Sigma-Aldrich-324523), and sodium acetate-d3 (Sigma-Aldrich) were administered via intraperitoneal injection and dosed at 2 g/kg (20% solution in saline, filtered through a Stericup GV filter). Conditioned place preference (CPP) was performed according to Cunningham et al³⁵. Briefly, Ugo Basile (Italy) mouse CPP boxes (Model Number: 42553) with external dimensions 35×18×29cm were used. The apparatus was divided into two chambers (16×15×25cm) that differed in wall and floor pattern. Striped walls were paired with circle cutouts (1 cm) and solid gray walls were paired with square cutouts (0.5 cm). Sessions were run in a dark room at ambient temperature. Boxes were cleaned with 70% ethanol between animals and allowed to dry between rounds. The paradigm consisted of 1 habituation day (5 min exploration in neutral environment), 1 pre-training session (20 min with access to both chambers), 8 training days (biased subject assignment, alternating sessions of saline or ethanol i.p. immediately prior to 5 min session) and 1 post-training test session (20 min with access to both chambers). Percent time spent in conditioned chamber was measured. Preference scores were calculated as the difference between time spent in conditioned chamber and unconditioned chamber. Shapiro-Wilks test was used to assess normal distribution and Mann-Whitney test to determine learning.

Intracranial injection of viral vector

Adult male C57BL/6J mice of 10 weeks of age were anaesthetized with isoflurane gas (1–5% to maintain surgical plane) and placed in a sterile field within a stereotaxic device. Artificial tears were applied to eyes to ensure sufficient lubrication. Animals received an injection of bupivacaine (2.5 mg kg⁻¹) for local anaesthesia before the skin was disinfected with betadine solution and the skull exposed with a short incision using sterile surgical equipment. A small hole (about 0.5 mm) was drilled in the skull over the target area using a stereotax and a stereotactic drill. A micro-syringe filled with viral vector was inserted into the dorsal hippocampus and slowly removed following injection (AP, – 2.0 mm; DV, – 1.4

mm; ML, \pm 1.5 mm from bregma). ACSS2 knockdown vector, AAV2/9; U6.shACSS2.CMV.EGFP. All animals received a single dose of subcutaneous meloxicam (5 mg/kg) as analgesia at induction and one dose per day for two days postoperatively as needed.

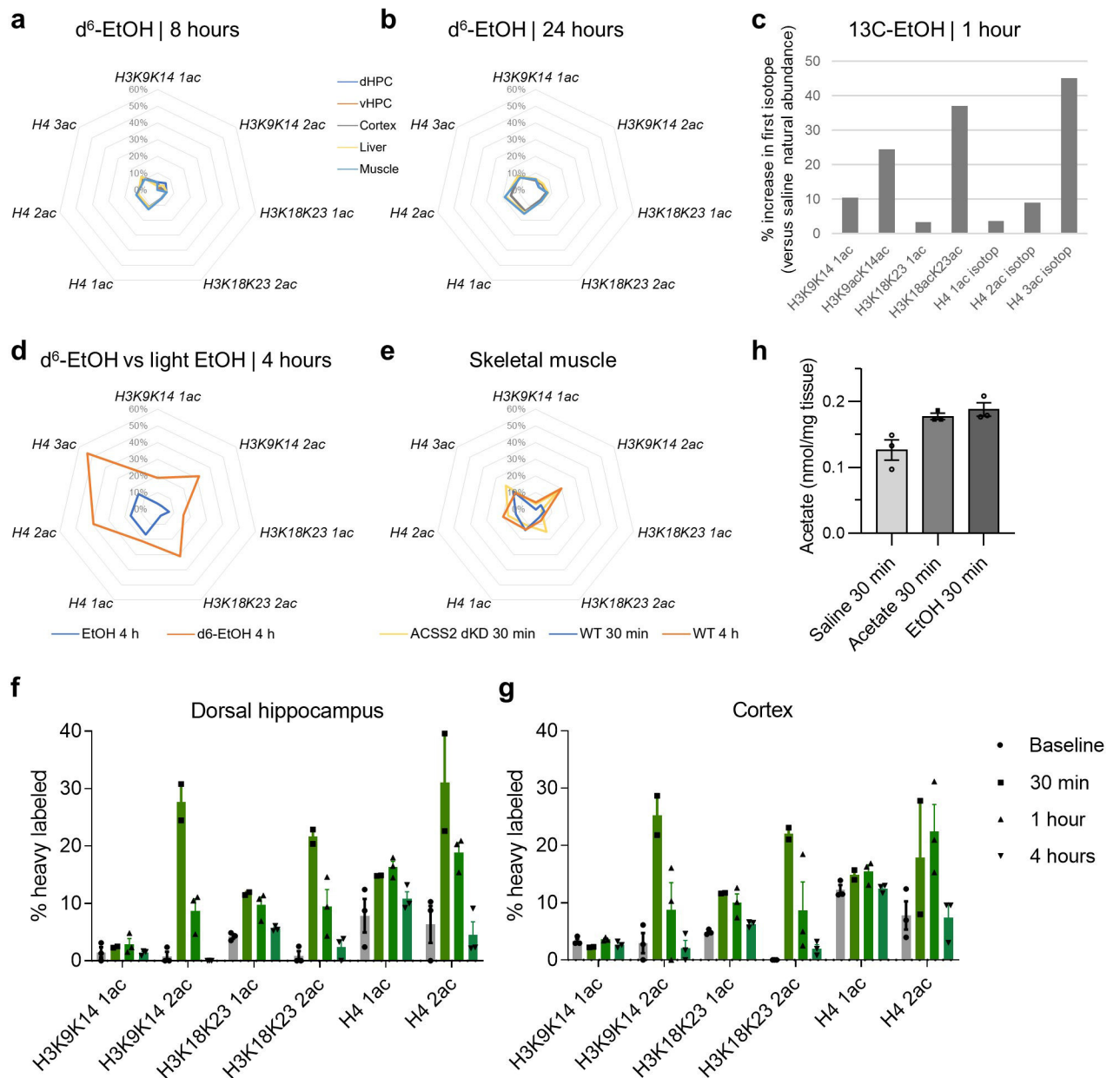
Extended Data



Extended Data Figure 1 |.

Ethanol-derived acetyl groups are rapidly incorporated into brain histone acetylation. **a**, Mass spec analysis of serum acetate shows rapidly increasing levels of acetate in alcohol-injected animals, at 30 minutes post-injection ($n = 3$ for saline, $n = 4$ for acetate group; data are mean \pm s.e.m., two-tailed unpaired T test, $P = 0.0258$). **b**, d6-EtOH is readily metabolized and thus labels blood acetate pools (d3-acetate detected by mass spec, $n = 4$ per group; data are mean \pm s.e.m., two-tailed unpaired T test, $P = 0.0016$). **c**, d6-EtOH label incorporation into cortical histone acetylation shows a similar pattern to the hippocampus.

The Arachne plot axis represents the % of the third isotope for the acetylated peptide, corresponding to the D₃ labeled form; the natural relative abundance of that isotope is apparent in the 'none' and 'saline 1h' treatment groups. **d**, Histone acetylation is relatively independent of alcohol metabolism in skeletal muscle, a tissue with low expression of ACSS2. **e, f**, Mass spectra (representative from three biological replicates) showing the relative abundance of deuterated histone H4-triacetyl peptide (aa 4–17) in hippocampus of wild-type mice at baseline and 4 hours following d6-EtOH injection. Increases of the M+1 (blue lines), M+2 (green lines) and M+3 (red lines) isotopes are shown in (e) and indicate a major increase of M+3. The contribution of singly (orange), doubly (grey) and triply (yellow) deuterated peptides to the isotopic distribution is shown in (f). The relative abundance of the M+3 isotope is increased about 6-fold at 4 hours following d6-EtOH injection, and is overwhelming due to the triply deuterated peptides; in comparison, the contribution of singly and doubly deuterated peptides to the M+3 isotope is minimal. The experiment was performed with 3 biological replicates per group. **g**, The relative abundance of the first four isotopes of each of the seven peptides in the untreated samples corresponds to the theoretical isotopic distribution of the peptides (calculated using envIPat²⁹; samples not treated with d6-EtOH n = 20 data are mean ± s.d.). **h**, Natural abundance-corrected contribution of M+1, M+2 and M+3 isotopes to histone acetylation labeling in liver and hippocampus following i.p. injection of d6-ethanol (calculated using FluxFix³⁰; n = 3 per group; data are mean ± s.d.).

**Extended Data Figure 2 |.**

Dynamics of ethanol and acetate-induced heavy label incorporation. **a, b**, Relative abundance of deuterated histone acetylation in dorsal Hippocampus (dHPC), ventral Hippocampus (vHPC), Cortex, Liver, and Muscle at 8 hours (a) and at 24 hours (b) after i.p. injection of d⁶-EtOH. **c**, C¹³-EtOH (carbon 1 heavy labeled) introduced via intraperitoneal injection readily labels hippocampal histone acetylation (% increase over natural abundance of ¹³C acetyl groups in saline-injected animals, $n = 1$). **d**, In contrast to heavy d⁶-EtOH, non-labeled EtOH control does not increase the natural abundance of heavy histone acetylation in the hippocampus. **e**, Histone acetylation is relatively independent of liver alcohol metabolism in skeletal muscle. Relative abundance of deuterated histone acetylation in skeletal muscle tissue at 30 minutes and 4 hours in WT mice, and 30 minutes in

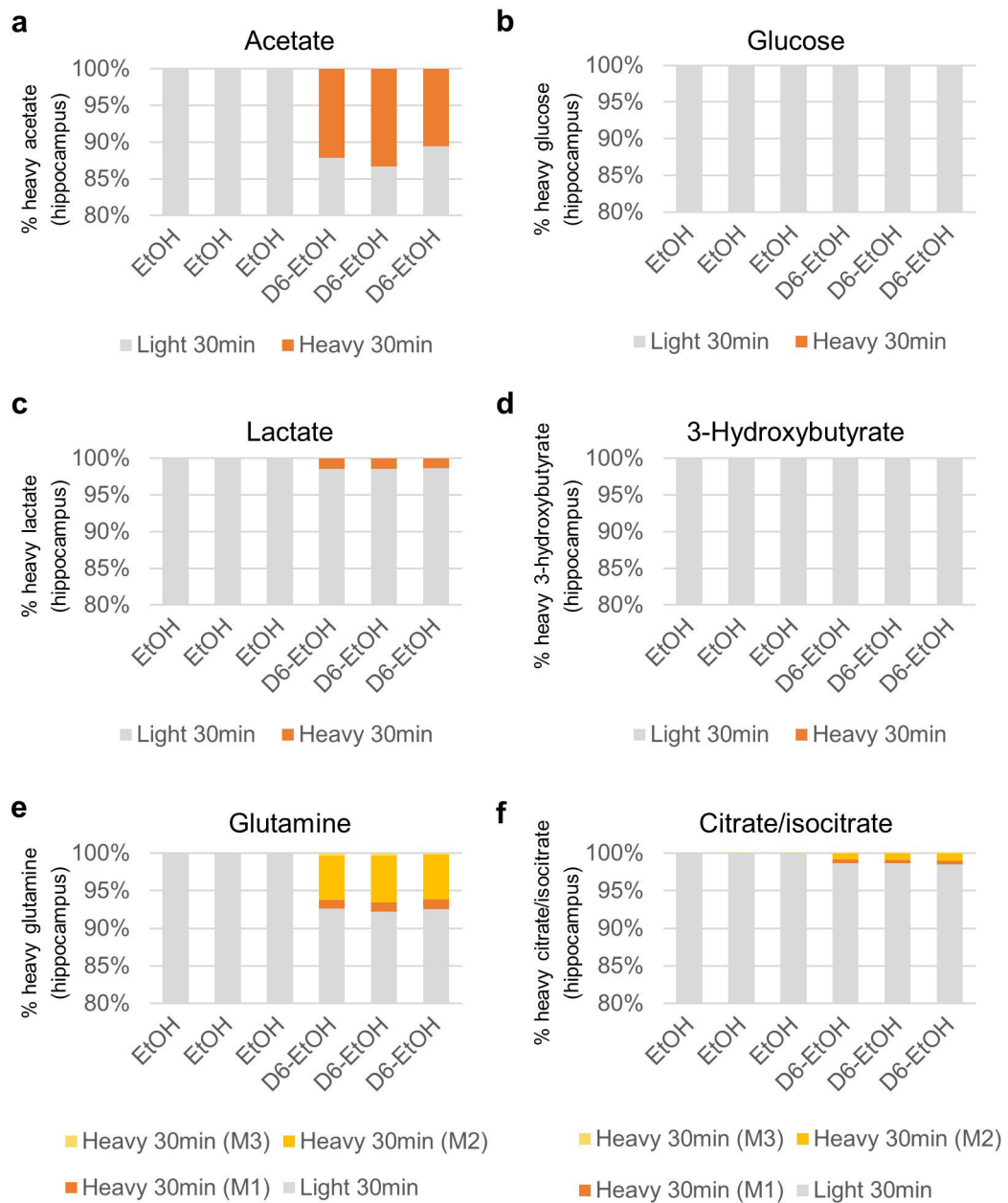
hippocampal ACSS2 KD mice. **f, g**, Heavy acetate introduced via intraperitoneal injection readily labels histone acetylation in the dorsal hippocampus (f), and in the cortex (g). ($n = 2$ at 30 min, $n = 3$ per group at other time points; data are mean \pm s.e.m.). **h**, Acetate levels measured mass spec in hippocampal tissue following acetate and ethanol injections ($n = 3$ per group; data are mean \pm s.e.m., two-tailed unpaired T test, 30min Acetate vs. Saline, $P = 0.0335$; two-tailed unpaired T test, 30 min EtOH vs. saline, $P = 0.0285$).

Author Manuscript

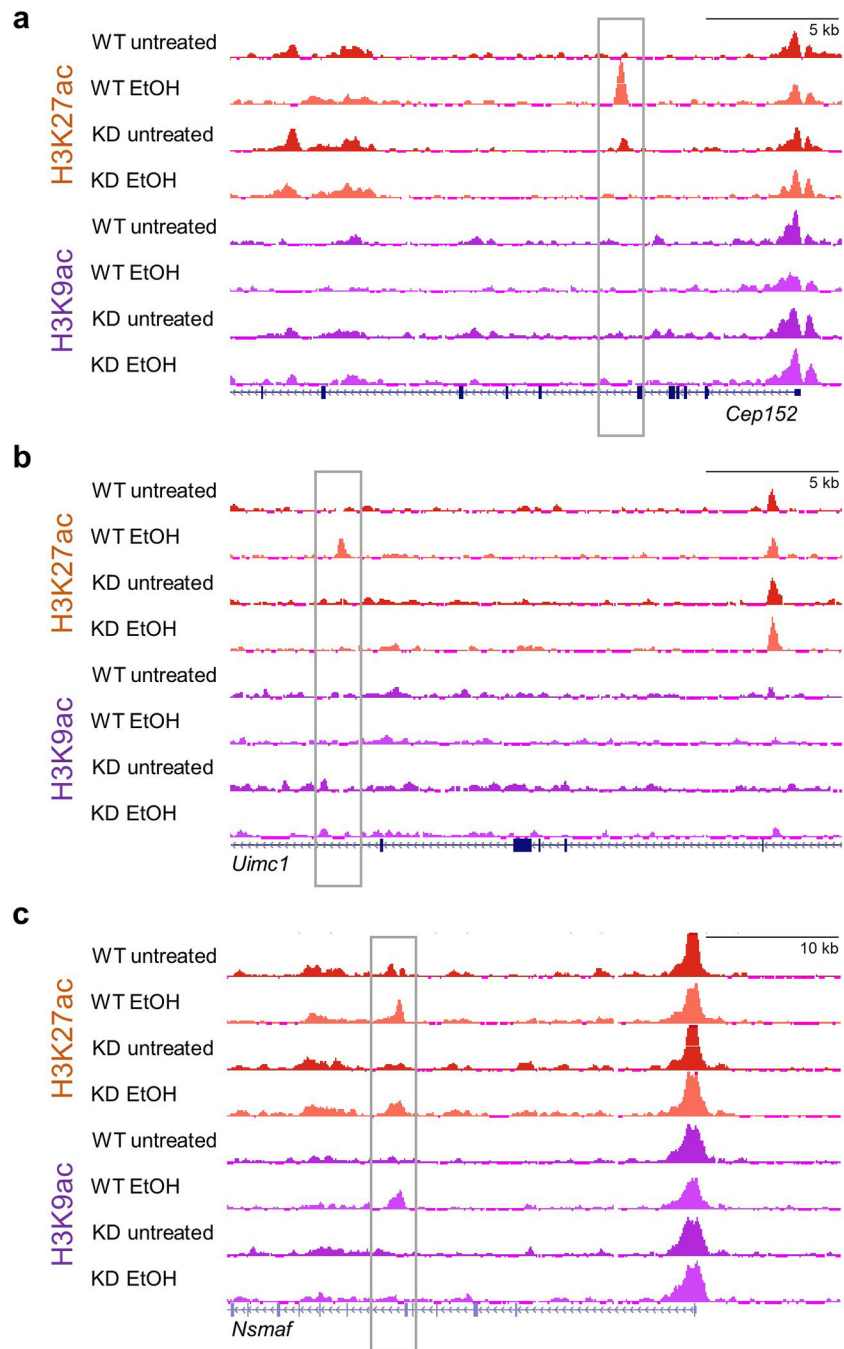
Author Manuscript

Author Manuscript

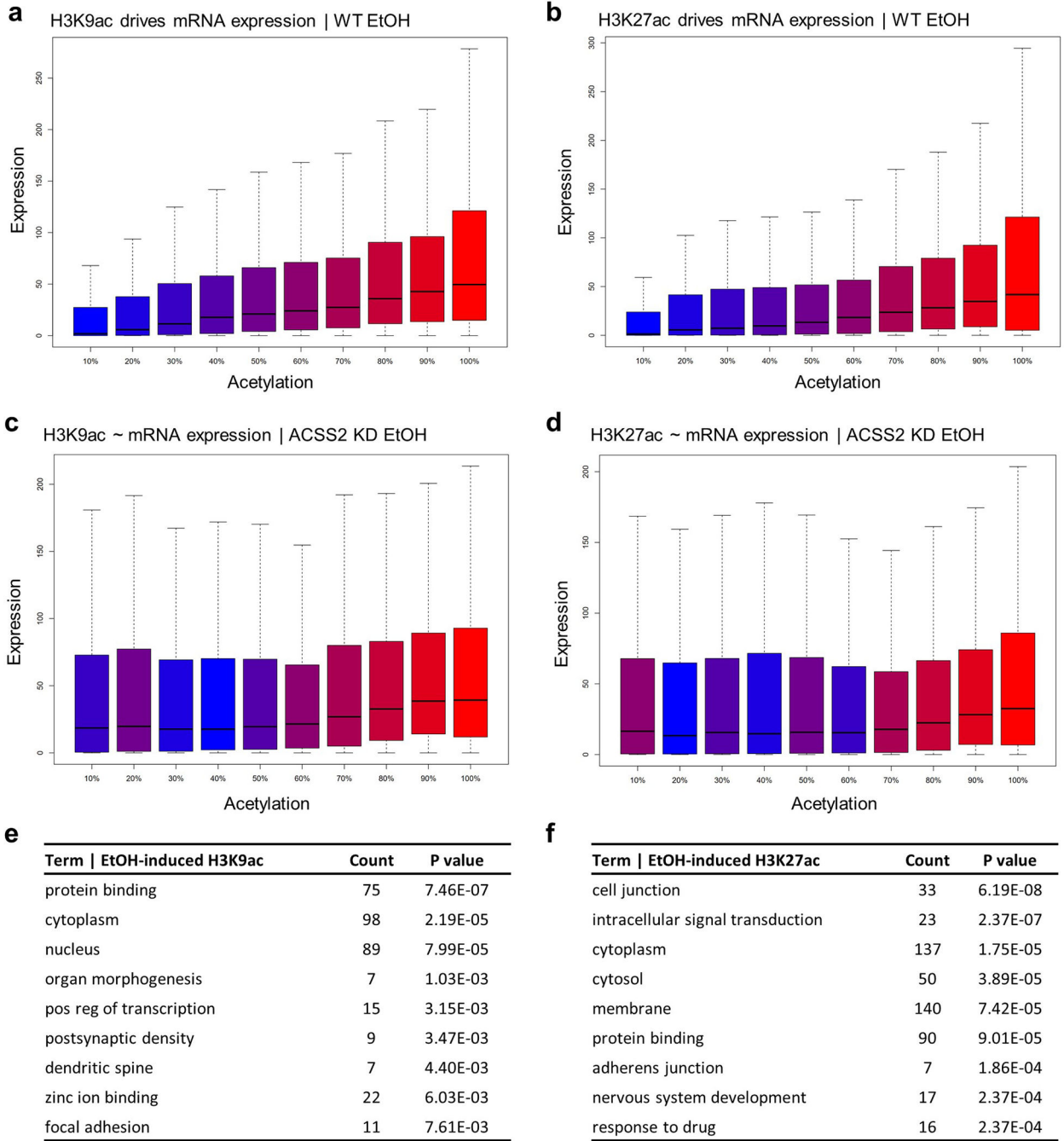
Author Manuscript

**Extended Data Figure 3 |.**

Metabolite labeling in hippocampal tissue 30 min following *i.p.* d6-EtOH injection. **a-f**, Mass spec quantification of metabolite labeling in hippocampal tissue at 30 minutes following *i.p.* d6-EtOH injection. d6-EtOH label was incorporated into hippocampal acetate pools (a). In contrast, d6-EtOH did not contribute to glucose pool (b) not to 3-hydroxybutyrate (d) in hippocampus, and only minimally to lactate (c). Labeling of 3-Hydroxybutyrate was not observed, in contrast to hippocampal Glutamine (e) and Isocitrate/Citrate (f) pools.

**Extended Data Figure 4 |.**

Representative H3K9ac and H3K27ac dorsal hippocampal ChIPseq tracks in control and EtOH-treated wild-type and ACSS2 knock-down mice. **a-c**, ChIP-seq for H3K9ac and H3K27ac in untreated and EtOH-treated WT and ACSS2 KD animals. Genome-browser track views show the (a) *Cep152* gene locus (Chr2:125,603,000–125,626,000), (b) *Uimc1* gene locus (Chr5: 55,064,000–55,089,000), and (c) *Nsmf* gene locus (Chr4: 6,425,000–6,464,000). The experiment was performed with 3 independent biological replicates per group.



Extended Data Figure 5 |.

Dorsal hippocampal epigenetic and transcriptional changes in control and EtOH-treated wild-type and ACSS2 knock-down mice. **a-d**, Decile plots of genes enriched in H3K9ac (a) and H3K27ac (b) show correlation with mRNA expression levels in hippocampus, in WT animals 1 hour following injection with EtOH. In contrast, in ACSS2 KD animals, the correlation between histone H3K9 acetylation (c) and H3K27 acetylation (d) and alcohol-related mRNA expression is largely lost (box-and-whisker plots show median value with whiskers extending to 1.5x the interquartile range; n = 16,553 genes (population) arranged

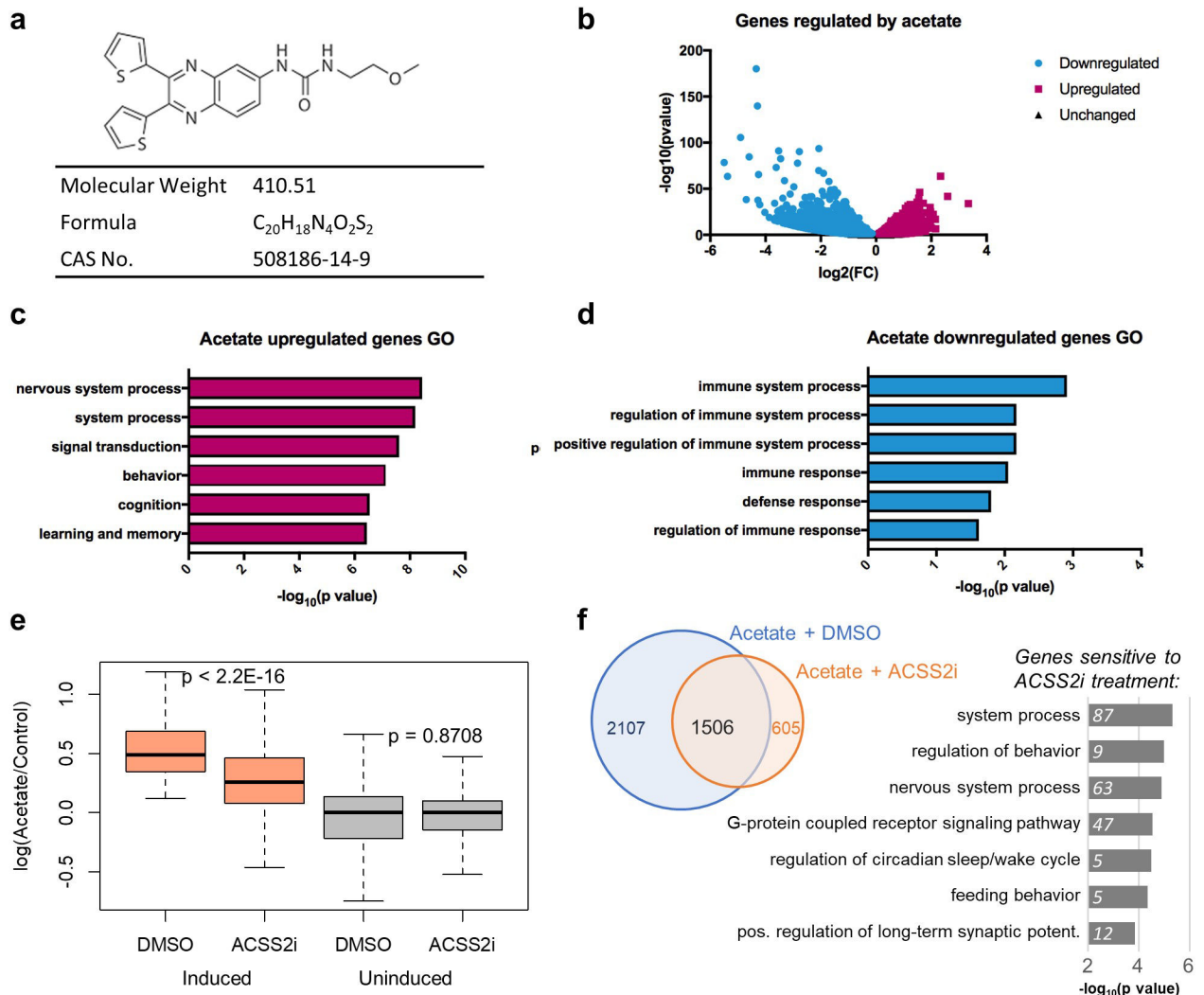
into ten equal-sized deciles by acetylation ChIP-seq enrichment) **e-f**, GO analysis on H3K9ac/H3K27ac peaks that are induced by EtOH in WT but not ACSS2 KD animals (n = 332 H3K9ac peaks and n = 480 H3K27ac peaks; Gene Ontology enrichment analysis performed using a modified Fisher's exact test (EASE) with the FDR controlled by the Yekutieli procedure, $-\log_{10}$ of nominal P values are shown).

Author Manuscript

Author Manuscript

Author Manuscript

Author Manuscript



Extended Data Figure 6 |.

Transcriptional changes in primary hippocampal neurons treated with supraphysiological levels of acetate. **a**, ACSS2i structure (C₂₀H₁₈N₄O₂S₂) **b**, RNAseq showing differentially regulated genes in primary hippocampal neurons treated with 5 mM acetate ($n = 4$ replicates per group; volcano plot of likelihood ratio test employed by DESeq2 (two-sided), FDR controlled for multiple hypothesis testing). **c,d**, Gene ontology (GO) analysis of significantly upregulated (**c**) ($n = 3613$ genes) and significantly downregulated (**d**) ($n = 3987$ genes) genes (GO analysis performed with GOrilla, using a minimal hypergeometric test). **e**, RNA-seq in primary hippocampal neurons isolated from C57/B16 mouse embryos and treated with acetate (5 mM) in the presence or absence of a small molecular inhibitor of ACSS2 (ACSS2i). 2107 of the 3613 acetate-induced genes fail to be upregulated in the presence of ACSS2i (box-and-whisker plots show median value with whiskers extending to 1.5x the interquartile range; $n = 3,613$ induced genes (population) or 3,613 randomly sampled genes (population) tested using two-sided Mann-Whitney rank-sum test, $P < 2.2E-16$). **f**, Shown in blue are acetate-induced genes in primary hippocampal neurons, together with the GO term analysis of ACSS2i sensitive genes (non-overlapping with yellow, which represents the

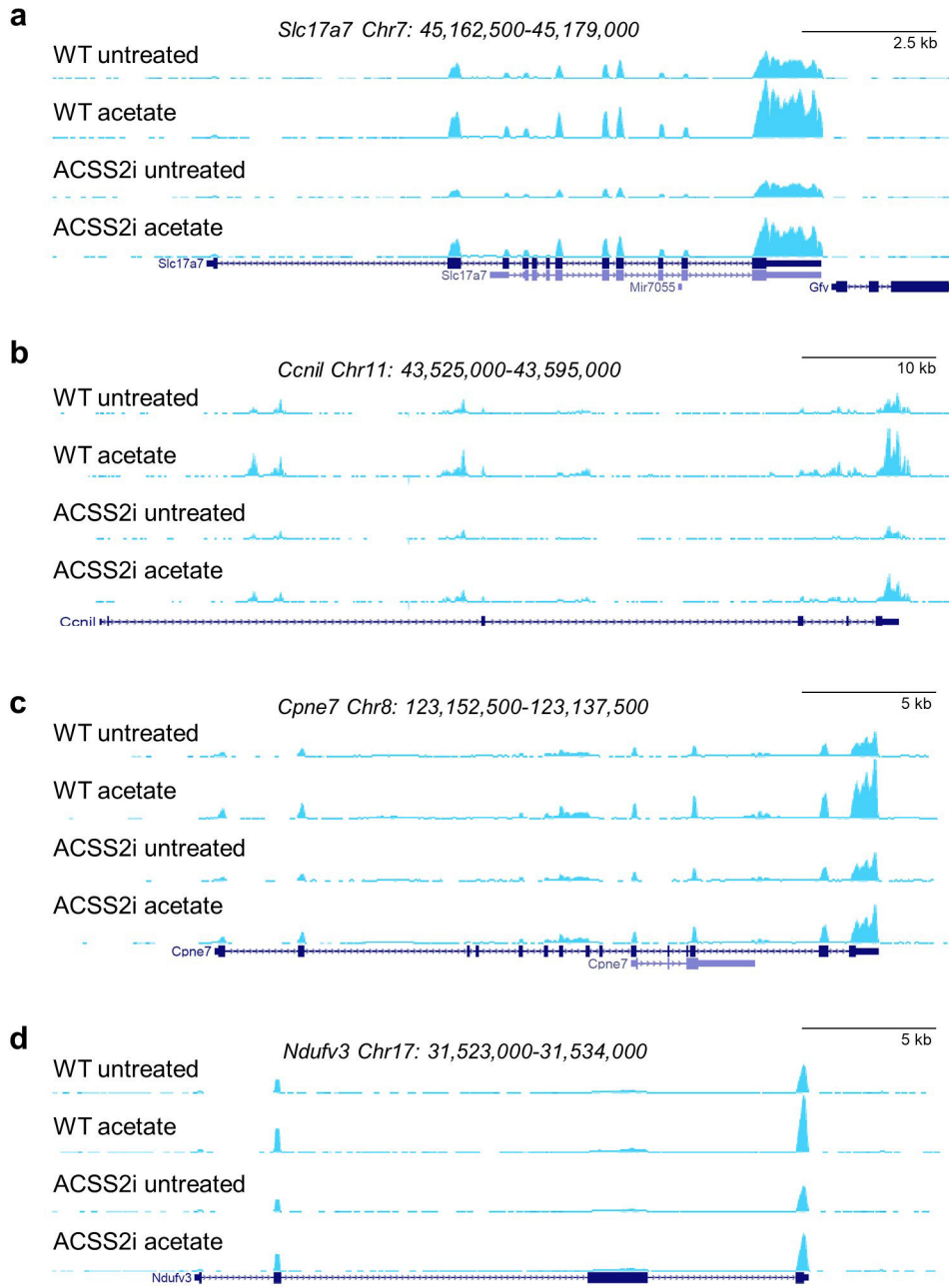
genes that are upregulated by acetate in the presence of ACSS2i; n = 2107, Gene Ontology enrichment analysis performed using a modified Fisher's exact test (EASE) with the FDR controlled by the Yekutieli procedure, $-\log_{10}$ of nominal P values are shown).

Author Manuscript

Author Manuscript

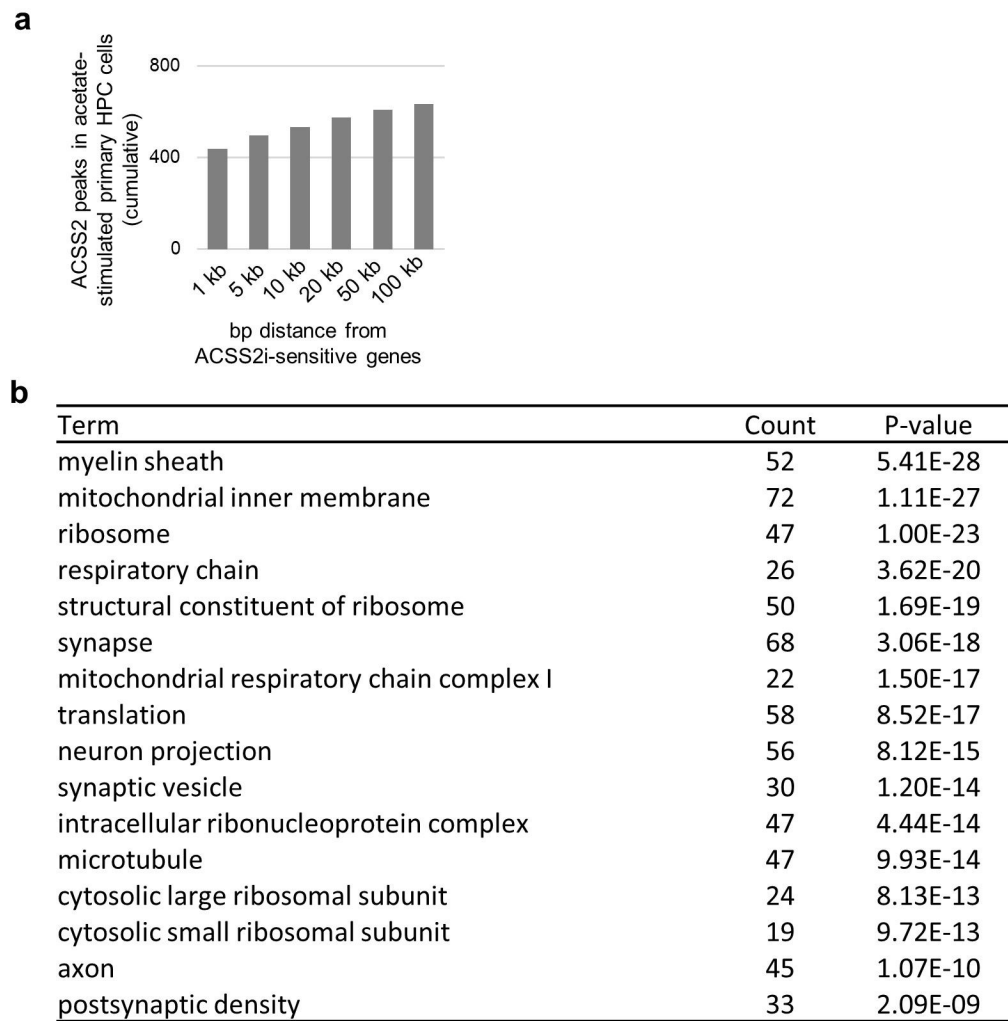
Author Manuscript

Author Manuscript



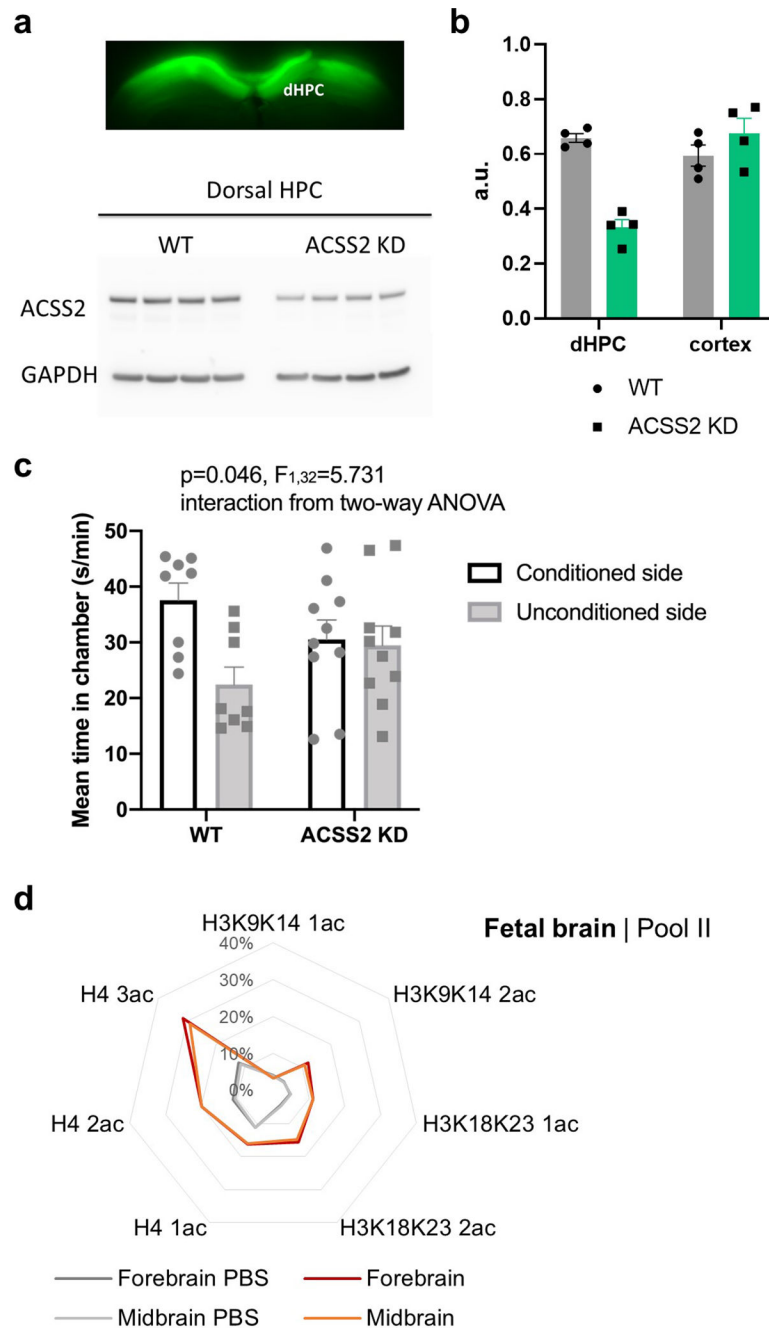
Extended Data Figure 7 |.

Representative RNA-seq tracks in control and acetate-treated primary hippocampal neurons in the presence or absence of ACSS2 inhibitors. **a-d**, Genome-browser track views showing examples of gene up-regulation upon acetate treatment in hippocampal neurons, and diminished induction with ACSS2i treatment ($n = 4$ per cohort). RNA-seq track views show the (a) *Slc17a7* gene locus (Chr7: 45,162,500–45,179,000), the (b) *Ccnil* gene locus (Chr11: 43,525,000–43,595,000), the (c) the *Cpne7* gene locus (Chr8: 123,152,500–123,137,500), and the (d) *Ndufv3* gene locus (Chr17: 31,523,000–31,534,000).



Extended Data Figure 8 |.

Acetate-induced transcriptional changes in primary hippocampal neurons relate to *in vivo* ACSS2 peaks and *in vivo* gene expression changes induced by ethanol. **a**, Cumulative number of ACSS2 peaks near the transcription start site (TSS) of acetylated ACSS2i sensitive genes, indicating that the majority ACSS2 binding events occurs over or proximal to the gene promoter. **b**, GO analysis for the 830 overlapping genes between the *in vivo* RNA-seq and *ex vivo* hippocampal neuron RNAseq (n = 830 genes (population), Gene Ontology enrichment analysis performed using a modified Fisher's exact test (EASE) with the FDR controlled by the Yekutieli procedure).

**Extended Data Figure 9 |.**

Behavioral importance of dorsal hippocampal ACSS2 expression and heavy label incorporation in the fetal brain. **a**, Representative image showing virus localization to the dorsal hippocampus (dHPC) and Western blot ($n = 4$ animals) showing dHPC ACSS2 levels in WT and ACSS2 KD mice (a.u. – arbitrary units; for gel source data, see Supplementary Figure 1). **b**, Quantification of ACSS2 protein levels in the dHPC and cortex of WT and dHPC ACSS2 KD mice ($n = 4$ animals; data are mean \pm s.e.m., multiple T test, dHPC ACSS2 KD vs. WT, $P = 0.0001$, q value = 0.0001; Cortex ACSS2 KD vs. WT, $P = 0.2666$, q value = 0.1347). **c**, ACSS2 is required for alcohol-induced associative learning. Mean time

(seconds/minute) spent in unconditioned and ethanol-conditioned chambers following ethanol-induced conditioned place preference training in WT ($n = 8$) and dorsal hippocampal ACSS2 knock-down mice ($n = 10$). Bar graphs represent mean \pm s.e.m. and show data points corresponding to individual animals. **d**, Heavy label incorporation into histone acetylation in the fetal brain. Data represent the second of two pools of embryos ($n = 4$ per pool) from maternal d6-EtOH injection. The Arachne plot axes represent the percentage of the third isotope of the acetylated peptide, corresponding to the D₃ labeled form.

Supplementary Material

Refer to Web version on PubMed Central for supplementary material.

Acknowledgments

We thank the Metabolomics Core of the Diabetes Research Center (DRC) for providing the metabolite mass spec quantification, and Dr. Joshua D. Rabinowitz, Princeton Metabolomics Core director, as well as Dr. Cholsoon Jang for valued advice. We thank the NeuronsRUs core of the Mahoney Institute for Neurological Sciences for preparations of primary hippocampal neurons. We especially acknowledge Dr. John Whetstone for valuable suggestion to test whether alcohol administration in a pregnant female mouse leads to histone acetylation in gestating fetal brain. G.E. was supported by The Brody Family Medical Trust Fund Fellowship in Incurable Diseases of The Philadelphia Foundation. This work was supported by NIH P01AG031862 and NIH R01AA027202.

References

1. Li X, Egervari G, Wang Y, Berger SL & Lu Z Regulation of chromatin and gene expression by metabolic enzymes and metabolites. *Nature Reviews Molecular Cell Biology* (2018). doi:10.1038/s41580-018-0029-7
2. Mews P et al. Acetyl-CoA synthetase regulates histone acetylation and hippocampal memory. *Nature* 546, 381–386 (2017). [PubMed: 28562591]
3. Sarkola T, Iles MR, Kohlenberg-Mueller K & Eriksson CJP Ethanol, acetaldehyde, acetate, and lactate levels after alcohol intake in white men and women: effect of 4-methylpyrazole. *Alcohol. Clin. Exp. Res.* 26, 239–245 (2002). [PubMed: 11964564]
4. Soliman ML & Rosenberger T a. Acetate supplementation increases brain histone acetylation and inhibits histone deacetylase activity and expression. *Mol. Cell. Biochem.* 352, 173–80 (2011). [PubMed: 21359531]
5. Pandey SC, Kyzar EJ & Zhang H Epigenetic basis of the dark side of alcohol addiction. *Neuropharmacology* 122, 74–84 (2017). [PubMed: 28174112]
6. Mews P & Berger SL Exploring the Dynamic Relationship Between Cellular Metabolism and Chromatin Structure Using SILAC-Mass Spec and ChIP-Sequencing. in *Methods in Enzymology* 311–329 (2016). doi:10.1016/bs.mie.2016.04.002
7. Comerford S a et al. Acetate dependence of tumors. *Cell* 159, 1591–602 (2014). [PubMed: 25525877]
8. Zakhari S Alcohol metabolism and epigenetics changes. *Alcohol Res.* 35, 6–16 (2013). [PubMed: 24313160]
9. Bonthuis PJ et al. Noncanonical genomic imprinting effects in offspring. *Cell Rep.* 12, 979–991 (2015). [PubMed: 26235621]
10. Zimatkin SM, Pronko SP, Vasiliou V, Gonzalez FJ & Deitrich RA Enzymatic mechanisms of ethanol oxidation in the brain. *Alcohol. Clin. Exp. Res.* 30, 1500–1505 (2006). [PubMed: 16930212]
11. Liu R et al. Fstl1 is involved in the regulation of radial glial scaffold development. *Mol. Brain* (2015). doi:10.1186/s13041-015-0144-8

12. Kalay E et al. CEP152 is a genome maintenance protein disrupted in Seckel syndrome. *Nat. Genet.* (2011). doi:10.1038/ng.725
13. Stessman HAF et al. Targeted sequencing identifies 91 neurodevelopmental-disorder risk genes with autism and developmental-disability biases. *Nat. Genet.* (2017). doi:10.1038/ng.3792
14. Volkow ND et al. Acute alcohol intoxication decreases glucose metabolism but increases acetate uptake in the human brain. *Neuroimage* 64, 277–83 (2013). [PubMed: 22947541]
15. Rao PSS, Bell RL, Engleman EA & Sari Y Targeting glutamate uptake to treat alcohol use disorders. *Frontiers in Neuroscience* (2015). doi:10.3389/fnins.2015.00144
16. Laufer BI et al. Associative DNA methylation changes in children with prenatal alcohol exposure. *Epigenomics* (2015). doi:10.2217/epi.15.60
17. Cates HM et al. Transcription Factor E2F3a in Nucleus Accumbens Affects Cocaine Action via Transcription and Alternative Splicing. *Biol. Psychiatry* 1–13 (2018). doi:10.1016/j.biopsych.2017.11.027
18. Stergiopoulos A & Politis PK Nuclear receptor NR5A2 controls neural stem cell fate decisions during development. *Nat. Commun.* 7, 1–16 (2016).
19. Mulligan MK et al. Molecular Profiles of Drinking Alcohol to Intoxication in C57BL/6J Mice. *Alcohol. Clin. Exp. Res.* 35, 659–670 (2011). [PubMed: 21223303]
20. Juarez B et al. Midbrain circuit regulation of individual alcohol drinking behaviors in mice. *Nat. Commun.* (2017). doi:10.1038/s41467-017-02365-8
21. Ferbinteanu J & McDonald RJ Dorsal/ventral hippocampus, fornix, and conditioned place preference. *Hippocampus* (2001). doi:10.1002/hipo.1036
22. Veazey KJ, Parnell SE, Miranda RC & Golding MC Dose-dependent alcohol-induced alterations in chromatin structure persist beyond the window of exposure and correlate with fetal alcohol syndrome birth defects. *Epigenetics Chromatin* 8, 39 (2015). [PubMed: 26421061]
23. Mead EA & Sarkar DK Fetal alcohol spectrum disorders and their transmission through genetic and epigenetic mechanisms. *Frontiers in Genetics* 5, (2014).
24. Mandal C, Halder D, Jung KH & Chai YG In utero alcohol exposure and the alteration of histone marks in the developing fetus: An epigenetic phenomenon of maternal drinking. *International Journal of Biological Sciences* 13, 1100–1108 (2017). [PubMed: 29104501]
25. Mews P & Calipari ES Cross-talk between the epigenome and neural circuits in drug addiction. in *Progress in Brain Research* 235, 19–63 (2017). [PubMed: 29054289]
26. Egervari G, Ciccocioppo R, Jentsch JD & Hurd YL Shaping vulnerability to addiction – the contribution of behavior, neural circuits and molecular mechanisms. *Neuroscience and Biobehavioral Reviews* 85, 117–125 (2018). [PubMed: 28571877]
27. Kriss CL et al. In Vivo Metabolic Tracing Demonstrates the Site-Specific Contribution of Hepatic Ethanol Metabolism to Histone Acetylation. *Alcohol. Clin. Exp. Res.* (2018). doi:10.1111/acer.13843
28. Linderstromlang K Deuterium exchange between peptides and water *Chemistry & Industry*. No. 18. 14 Belgrave Square, London SW1X 8PS, Soc Chemical Industry, (1955). No Title.
29. Loos M, Gerber C, Corona F, Hollender J & Singer H Accelerated isotope fine structure calculation using pruned transition trees. *Anal. Chem.* (2015). doi:10.1021/acs.analchem.5b00941
30. Trefely S, Ashwell P & Snyder NW FluxFix: Automatic isotopologue normalization for metabolic tracer analysis. *BMC Bioinformatics* (2016). doi:10.1186/s12859-016-1360-7
31. Feroandez CA, Rosiers C Des, Previs SF, David F & Brunengrabert H Correction of 3C Mass Isotopomer Distributions for Natural Stable Isotope Abundance. 31, 255–262 (1996).
32. Nativio R, et al. Dysregulation of the epigenetic landscape of normal aging in Alzheimer’s disease. *Nat. Neurosci.* (2018). doi:10.1038/s41593-018-0101-9
33. Langmead B & Salzberg SL Fast gapped-read alignment with Bowtie 2. *Nat. Methods* (2012). doi: 10.1038/nmeth.1923
34. Chen X et al. Integration of External Signaling Pathways with the Core Transcriptional Network in Embryonic Stem Cells. *Cell* (2008). doi:10.1016/j.cell.2008.04.043
35. Cunningham CL, Gremel CM & Groblewski PA Drug-induced conditioned place preference and aversion in mice. *Nat. Protoc.* (2006). doi:10.1038/nprot.2006.279

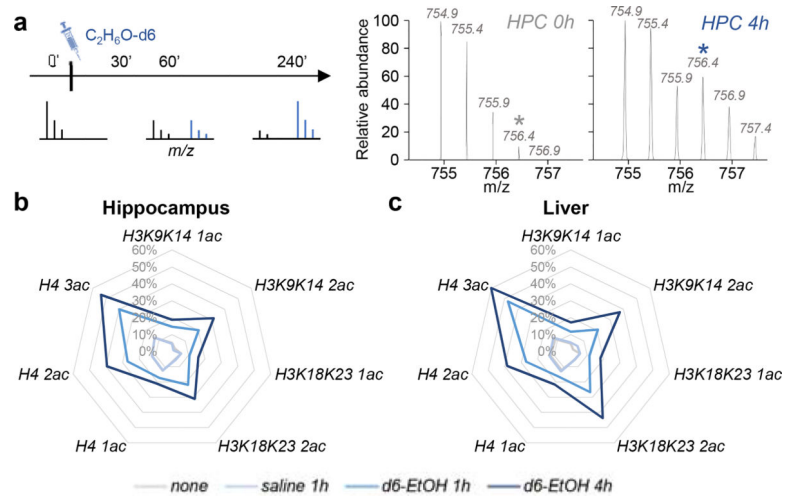


Figure 1 |.

Alcohol metabolites feed histone acetylation in the brain. **a**, Experimental outline of *in vivo* d6-EtOH mass spectrometry. **b**, Metabolized heavy d6-EtOH is incorporated into histone acetylation in hippocampus. The Arachne plot axis represents the % of the third isotope for the acetylated peptide, corresponding to the D₃ labeled form; the natural relative abundance of that isotope is apparent in the ‘none’ and ‘saline 1h’ treatment groups. **c**, Label incorporation into histone acetylation occurs earlier in the liver, the principal site of alcohol metabolism.

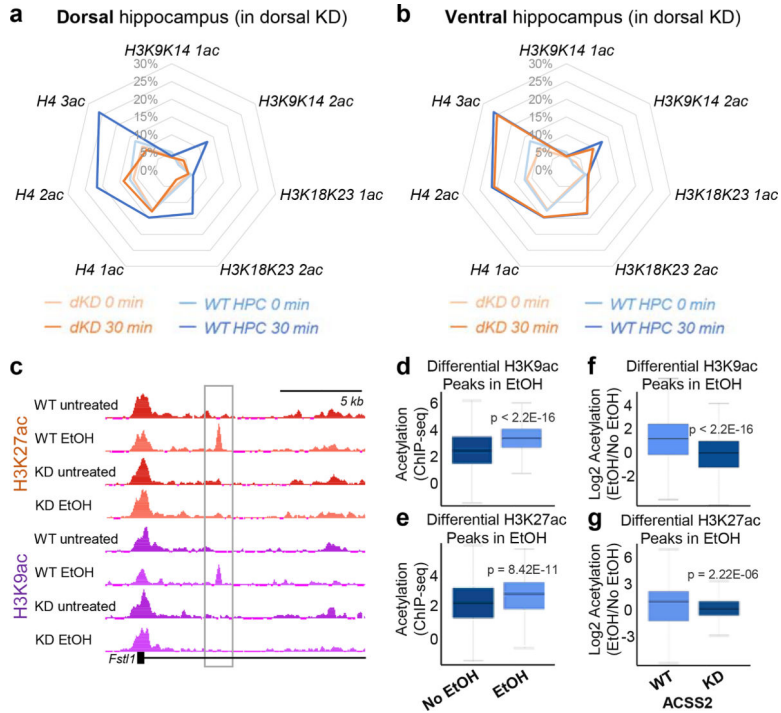


Figure 2 |. Mass spectrometry analysis of d6-EtOH in dHPC ACSS2 KD. **a**, Knockdown of ACSS2 expression in dorsal hippocampus prevents incorporation of the heavy label into histone acetylation. **b**, In the same animal, incorporation of the heavy label in the ventral hippocampus (where ACSS2 levels are normal) is not changed when compared to control mice. **c**, ChIP-seq for H3K9ac and H3K27ac in untreated and EtOH-treated WT and ACSS2 KD animals ($n = 3$ independent replicates). Genome-browser track view shows the *Fstl1* gene locus (Chr16: 37,776,000–37,793,000). **d**, **e**, ChIP-seq for H3K9ac (**d**) and H3K27ac (**e**) *in vivo* shows increased acetylation genome-wide following EtOH injection (339/458 H3K9ac peaks, 490/816 H3K27ac peaks; called with MACS2, 10% FDR threshold DiffBind; box-and-whisker plots show the first and third quartile values and the median (center) value with whiskers extending to 1.5x the interquartile range; two-sided Mann-Whitney rank-sum test, $P < 2.2E-16$ (**d**), $P = 8.42e-11$ (**e**)). **f**, **g**, Induction of H3K9ac (**f**) and H3K27ac (**g**) is diminished in ACSS2 KD (458 H3K9ac peaks, 816 H3K27ac peaks; box-and-whisker plots show median value with whiskers extending to 1.5x the interquartile range; two-sided Mann-Whitney rank-sum test, P -value $< 2.2E-16$ (**f**), $P = 2.22e-6$ (**g**)).

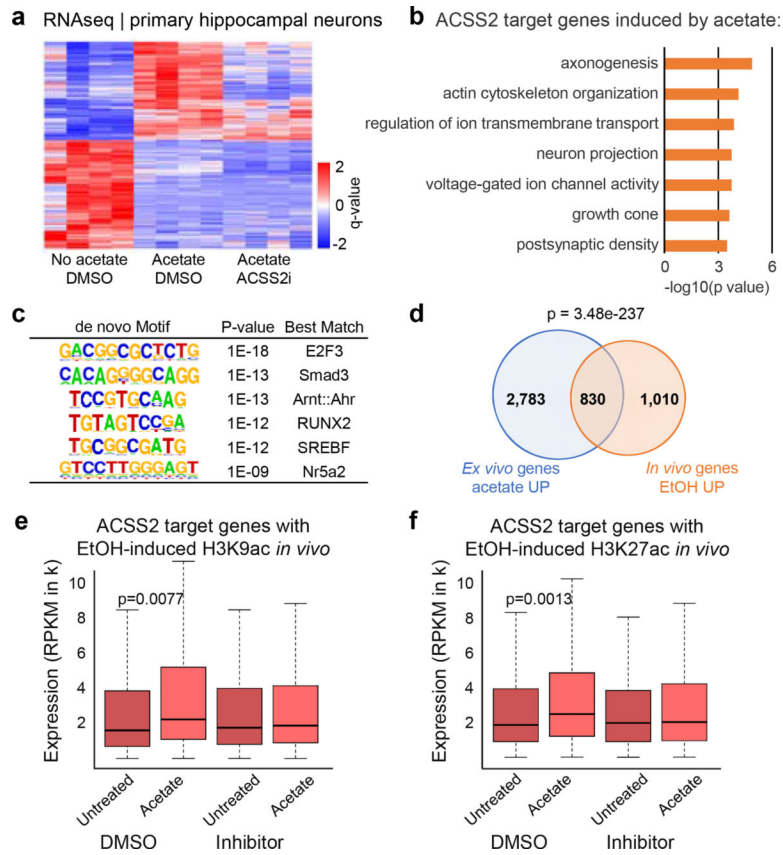


Figure 3 |.

ACSS2 mediated acetate-induced transcription in primary hippocampal neurons. **a**, RNA-seq in primary hippocampal neurons isolated from C57/Bl6 mouse embryos and treated with acetate (5 mM) in the presence or absence of a small molecular inhibitor of ACSS2 (ACSS2i). Heatmap showing 7,600 genes differentially expressed upon acetate treatment, and a third column showing the behavior of those genes under in the presence of the ACSS2 inhibitor. 2107 of the 3613 acetate-induced genes fail to be upregulated in the presence of ACSS2i ($n = 4$ per group). **b**, GO term analysis of genes that are *both* sensitive to acetate and directly bound by ACSS2 (from ACSS2 ChIP-seq; $n = 429$ genes, population assessment using modified Fisher's exact test (EASE) with the FDR corrected by the Yekutieli procedure, $-\log_{10}$ of nominal P values are shown). **c**, HOMER unsupervised *de novo* motif analysis of ACSS2 hippocampal binding sites targeting acetate-sensitive genes (*de novo* motif analysis of 751 ACSS2 peaks, hypergeometric test for each motif comparing background set of ACSS2 peaks that do not target acetate sensitive genes). **d**, Overlap of genes upregulated by EtOH *in vivo* (dHPC) and acetate *in vitro* ($n = 830$; hypergeometric test of gene set overlap, $P = 3.48e-237$). **e**, **f**, ACSS2 target genes with alcohol-induced H3K9ac (**e**) and H3K27ac (**f**) *in vivo* are upregulated by acetate in HPC neurons *in vitro*. ACSS2i blocks this gene induction (box-and-whisker plots show median value with whiskers extending to 1.5x the interquartile range; $n = 285$ genes (**e**) and $n = 362$ genes (**f**) tested against an equal number of control genes using two-sided Mann-Whitney rank-sum test; $P = 0.0077$ (**e**), $P = 0.0013$ (**f**)).

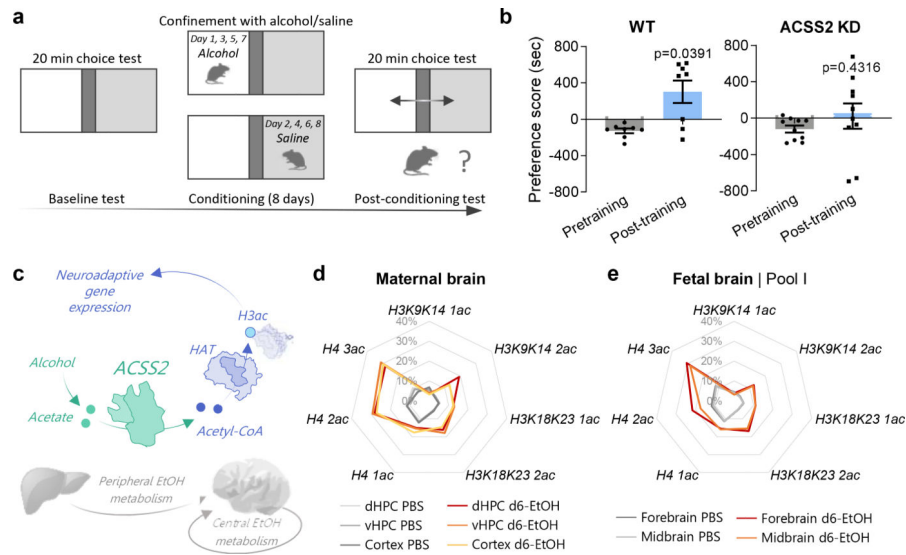


Figure 4 |.

ACSS2 is required for alcohol-induced associative learning. **a**, Schematic of ethanol-induced conditioned place preference (CPP). **b**, Preference scores for the ethanol-paired chamber in wild-type (WT) mice ($n = 8$; data are mean \pm s.e.m., Wilcoxon matched-pairs signed rank test, $P = 0.0391$) and for the ethanol-paired chamber in mice with dorsal hippocampal knock-down (KD) of ACSS2 ($n = 10$; data are mean \pm s.e.m., Wilcoxon matched-pairs signed rank test, $P = 0.4316$). **c**, Model. Acetate from hepatic alcohol breakdown is activated by neuronal ACSS2 in the brain and readily induces gene-regulatory histone acetylation. **d**, Metabolized heavy d6-EtOH is incorporated into histone acetylation in the maternal brain. **e**, Heavy label incorporation into histone acetylation in the fetal brain. Data represent the second of two pools of embryos ($n = 4$ per pool) from maternal d6-EtOH injection. The Arachne plot axes represent the percentage of the third isotope of the acetylated peptide, corresponding to the D₃ labeled form.